Published in final edited form as:
Nanomedicine. 2015 January ; 11(1): 137–145. doi:10.1016/j.nano.2014.08.008.

Cellular Level Robotic Surgery: Nanodissection of Intermediate Filaments in Live Keratinocytes

Ruiguo Yang, PhD[a], **Bo Song, MEng**[a], **Zhiyong Sun, MEng**[a], **King Wai Chiu Lai, PhD**[b], **Carmen Kar Man Fung, PhD**[c], **Kevin C. Patterson, MD**[d], **Kristina Seiffert-Sinha, MD**[e], **Animesh A. Sinha, MD, PhD**[e,*], and **Ning Xi, DSc**[a,b,*]

[a]Department of Electrical and Computer Engineering, Michigan State University, East Lansing, MI USA, 48824

[b]Department of Mechanical and Biomedical Engineering, City University of Hong Kong, Hong Kong

[c]Hong Kong Productivity Council, Hong Kong

[d]College of Human Medicine, Michigan State University, East Lansing, MI, USA, 48824

[e]Department of Dermatology, University at Buffalo, Buffalo, NY, USA, 14203

Abstract

We present the nanosurgery on the cytoskeleton of live cells using AFM based nanorobotics to achieve adhesiolysis and mimic the effect of pathophysiological modulation of intercellular adhesion. Nanosurgery successfully severs the intermediate filament bundles and disrupts cell-cell adhesion similar to the desmosomal protein disassembly in autoimmune disease, or the cationic modulation of desmosome formation. Our nanomechanical analysis revealed that adhesion loss results in a decrease in cellular stiffness in both, the case of biochemical modulation of the desmosome junctions or mechanical disruption of intercellular adhesion, supporting the notion that intercellular adhesion through intermediate filaments anchors the cell structure as focal adhesion does and that intermediate filaments are integral components in cell mechanical integrity. The surgical process could potentially help reveal the mechanism of autoimmune pathology-induced cell-cell adhesion loss as well as its related pathways that lead to cell apoptosis.

Keywords

Atomic Force Microscopy; nanosurgery; intermediate filament; mechanical property; cell-cell adhesion; desmosome

Correspoding authors: Animesh A. Sinha, Department of Dermatology, University at Buffalo, NY, USA, 14203, Tel.: 716-204-5350, Fax: 716-204-5355, aasinha@buffalo.edu; Ning Xi, Department of Electrical and Computer Engineering, Michigan State University, East Lansing, MI, USA, 48824, Tel.: 517-4321925, Fax: 517-3551980, xin@egr.msu.edu.

The authors have no conflict of interest to declare.

Introduction

Surgery is a centuries-old medical technique that uses tissue/organ specific physical intervention to treat illness. Modern surgery has been taken to new levels with engineering technology that places robots at the center of operations to achieve higher precision, thus the name robotic surgery (1). Microsurgery has been successfully used on small blood vessels or nerves with dimensions of 1 mm^2. New technology has been pushing surgical precision to new limits. A new medical frontier looms in the horizon – surgery on cells, the smallest living unit, with precision down to the nanoscale and operation at the molecular level. Femto-second laser nanosurgery can achieve the desired non-invasiveness, only at the sub-micron resolution (2).

We have implemented Atomic force microscopy (AFM) as a surgical instrument to operate on living cells with resolution down to nanometers. AFM has been applied in investigations of biological processes with high resolution imaging and mechanical property characterization(3). With a sharp probe as its main imaging unit, it is naturally a surgery instrument at the nanoscale. AFM was first developed as an imaging instrument, and a number of biological samples have been visualized ranging from tissues, to cells, to cellular components, and even molecules with vertical resolution as high as an angstrom (4, 5). Imaging by AFM is the direct result of the scanning motion driven by the piezo actuation unit. To perform the nanosurgery, the position of the tip is not linearly related to applied signal and the applied voltage should be an arbitrary shape. Besides, most operations on biological samples are performed in liquid. Thus, the viscoelasticity of the sample requires a higher response frequency, and a nanorobotic system was developed to address these issues (6). Studies in cell biology have been taken to a whole new level with the introduction of AFM based nanorobotics. Equipped with the precision control capabilities, the nanorobot can have a workspace of nanoscale, but the controllability of a traditional robot. Thus, the handling of matters in the nanoscale would be achieved with stability, accuracy and efficiency. AFM nanorobotic systems allow human-directed position, velocity and force control with high frequency feedback. Most importantly, it can provide the operator with the real-time imaging of manipulation results from the fast-imaging based local scanning (7).

Researchers have reported on the dissection of DNA molecules, proteins, cell membranes, intermediate filaments, among other structures (8-12). Studies have shown the capability of AFM nanosurgery on fixed cell membranes by making incisions with a resolution of 100 nm or less (13, 14). Isolated gap junctions were dissected to resolve their detailed structures(12). In addition, isolated intermediate filaments were stretched with an AFM probe to test their tensile strength (15). At the current stage, most of these nanomanipulation experiments were performed to demonstrate the basic capability of AFM based nanomanipulation systems in handling and changing biological matters, since it remains challenging in controlling the tip-live cell interaction in living conditions. We report the use of nanorobotics for the nanodissection of cellular structures on living keratinocytes *in situ* to achieve adhesiolysis and to mimic the effect of pathophysiological modulations of intercellular adhesion.

Keratinocytes are the major component of the epidermis, or top layer of skin, and contains desmosome-based cell-cell adhesion structures. Desmosomes are cadherin based

intercellular junctions in epithelial cells to maintain their mechanical integrity and provide strength (16), acting like a “spot-welding” point connecting intermediate filaments from neighboring keratinocytes. The AFM images in Figure 1A and B captured the intermediate filaments underneath the cell membrane between neighboring cells. The structures agree well with the fluorescence images from the work published by Godsel and coworkers (17), in which the yellow dots display the desmosomal complexes surrounding cells at the periphery and the red shows the intermediate filaments. There is a narrow area a few hundred nanometers in length and approximately 50 nm in width when characterized by an electron microscope that comprises a cluster of proteins. Among them, trans-membrane desmosomal cadherins, desmogleins (Dsg) and desmocollins (Dsc) bind to the armadillo family protein plakoglobin (PG), which anchors the plakin family member desmoplakin (DP) and plakophilins (PKP) (18). The lateral interactions among these proteins allow tethering to intermediate filaments. Dsc molecules from neighboring cells form covalent bonds in a Ca^{2+} dependent manner.

Desmosomes are the target of autoimmune antibodies in several skin disorders, including pemphigus vulgaris (PV), in which intercellular adhesion is disrupted through disassembly of desmosomal proteins, especially Dsg3 (19). We have previously investigated the structural characterization of desmosomes in cultured keratinocytes lines and shown that the loss of intercellular adhesion via desmosomal disruption (20) can lead to mechanical property change (21). According to the cellular tensegrity model, the cell cytoskeleton is a tensional integrity structure bounded by the cell membrane, in which microtubules are the compressive element while actin filaments and intermediate filaments are tensional elements (22, 23). The structure bears most external forces on the cell and is able to maintain force balance through interaction with extracellular matrix (ECM), via mainly focal adhesions, serving as the anchoring point for the cell body (24, 25). Desmosomes link the intermediate filaments of neighboring cells through cell-cell adhesions, and the intermediate filaments are the tensional elements. Therefore, it is logical to consider the roles desmosomes play in the tensegrity structure.

In this study, we sought to investigate the integral role of desmosomes in maintaining the cellular structure by modulating the desmosome mechanically using nanosurgery. We applied the AFM based nanorobotic system to mechanically disrupt the intercellular adhesion to mimic the pathophysiological treatment. Nanosurgery successfully dissected the cellular connection by severing the intermediate filaments underneath the cell membrane. The biochemical and mechanical modulation were verified by AFM nanomechanical analysis which shows the decrease of cellular stiffness after the three mechanisms of modulation, indicating that the tension in the cytoskeleton structure was released by loss of intercellular connection. A mechanical model with struts and cables was derived to verify the experimental results. Our study demonstrates that cellular junctions, especially desmosomes, play an important role in providing the external support and anchoring just like focal adhesions do.

Methods

Cell line and reagents

The human keratinocyte cell line HaCaT was used in this study. Cells were grown in DMEM medium (Gibco-Invitrogen, Carlsbad, Ca) supplemented with 10% fetal calf 5 serum (Gemini Bio-products, West Sacramento, Ca) and 1% penicillin:streptomycin (10,000 U/ml:10,000 μg/ml; Gibco) at 37°C in a humidified atmosphere containing 5% CO_2.

The pathogenic anti-Dsg3 antibody Px4-3 isolated from a patient with mucocutaneous PV (kind gift from Dr. Aimee Payne, Department of Dermatology, University of Pennsylvania, Philadelphia, PA). The antibody was diluted in phosphate buffered saline (PBS) at 1:50 dilution.

AFM imaging and mechanical property characterization of HaCaT cells

HaCaT cells were cultured as described above until confluency. The cells were then seeded onto glass slides pretreated with poly-ornithine for attachment. The AFM imaging of live cells was performed on a modified Bioscope AFM (Bruker-Nano, Santa Barbara, CA) with a scanner of 90 μm by 90 μm lateral scan range. A silicon nitride AFM probe was used with a spring constant of 0.3 N/m calibrated by thermal tune method and a natural oscillation frequency of 18.5 kHz in liquid at TappingMode. All the imaging and mechanical measurements were performed as the cells on glass slides were immersed in cell culture solution inside a Petri dish. Temperature was maintained at 37°C throughout the entire experiment with a custom-made polyimide film-based heater.

Silicon nitride tips (Bruker-Nano, Santa Barbara, CA) with a spring constant of 0.3 N/m and a tip radius around 10 nm were used to probe the cells for elasticity. The collection of force-displacement curves was carried out under low frequency to ensure a low tip motion velocity as to minimize the dynamic effect. An indentation speed of 1.8 μm/s was selected to reduce the cell viscous effect but maintain a sufficient time frame to capture dynamic changes of cell properties. To ensure data reliability, all measurements were performed in the cell center. During this process, the indentation force was controlled below 10 nN and the indentation depth below 500 nm. Collected force-displacement curves were processed with Matlab routines to convert them to force-indentation curves and then fitted with the Hertzian model to generate the Young's modulus. The tip half opening angle is 17.5 degrees and the Poisson ratio was set as 0.5 for incompressible material.

AFM nanorobotic system for nanosurgery on live keratinocytes

The imaging of AFM is the direct result of the scanning motion driven by the XY direction piezo actuation unit. From the motion control perspective, the zigzag shaped driving voltage is applied to the XY piezo scanner, causing a linear motion back and forth with a pre-defined frequency. However, this is not the case for a nanomanipulation operation, where the position of the tip is not linearly related to applied signal and the applied voltage should be an arbitrary shape rather than a zigzag. Besides, most nanomanipulation operations on biological samples are performed in liquid. Thus, the viscoelasticity of the sample requires a higher response frequency, and the control system should be upgraded to meet this demand.

The upgraded hardware and software configurations convert a commercial AFM to a nanobiomanipulation oriented AFM. The technical details of the development of motion controller can be found in (26). In brief, we used a signal access module to provide all the signals needed for the external control of the manipulation operation by the Linux controller with data acquisition cards as the interface. The joystick is the command input where all the motions start, enabling the precision manipulation of nanoscale objects with force feedback.

Tensegrity model verifies the mechanical property change associated with cell adhesion loss

The tensegrity model is a qualitative model for adherent cells (22, 23) based on the concept that the cell body is a tensional integrity structure with prestress. The cytoskeleton behaves like a discrete mechanical network in which pre-stress is a major determinant of cell mechanics. Cells maintain force balance between microtubules, microfilaments and ECM, achieving equilibrium with internal tension, compression and their external support. Most believe that the internal tension is supported by the actin filaments and the intermediate filaments (when there is a large strain); while microtubules, normally stiffer than the other two cytoskeletal components, bear the compression. The external support comes from focal adhesions where integrins bind to the extracellular matrix.

The structure in Figure 2A with six struts (black) and 24 cables (blue) is developed by Stamenovic (27) as a conceptual model for cellular tensegrity. It is constructed by linking the ends of compressional struts with the tensional cables. The struts represent the microtubule while the cables denote the actin filaments. To quantify the relationship between the stress and the strain and to obtain the Young's modulus values, parallel loads are applied to both ends of the structure. A force of T/2 is applied to the nodes of C in Figure 2A. The structure with intermediate filament was designed according to the configurations of the intermediate filament in cells with the tensional elements projecting from the center to the peripheral illustrated in Figure 2B.

By virtual work method, we assume that the work of $\boldsymbol{T}$ on an incremental extension e per unit reference volume $\boldsymbol{V}$ of the model equals the work of uniaxial stress on the incremental change in uniaxial strain δ_{e_X}, that is $\frac{T\delta_{s_X}}{V}=\sigma_X\delta_{e_X}$. The volume enclosed by the structure is: $V=\frac{5L^3}{16}$. By definition: $\delta_{e_X}=\frac{\delta_{s_X}}{s}$, and the initial distance between parallel struts: $s_0=L_0/2$. Thus $\delta_{e_X}=\frac{2\delta_{s_X}}{L}$, and we have $\sigma_X=\frac{8T}{5L^2}$, so we have the derivative: $\frac{d\sigma_X}{ds_X}=\frac{8}{5L^2}\frac{dT}{ds_X}$. By definition: $E*=\frac{d\sigma_X}{de_X}$, thus the expression of E* can be obtained:

$$E*=\frac{4}{5L}\frac{d\sigma_X}{ds_X} \quad (1)$$

From equation (1) we know the Young's modulus E* of the structure in the form of equation (3) expressed in terms of the relationship between $\boldsymbol{T}$ and s_X . This could be defined for both

cases with and without the intermediate filament structures. Then the only remaining term is to find the relation between the force ***T*** and the distance between the struts s_X . For the configuration without the intermediate filaments, the calculation is as follows. The relationship between the force ***T*** and the extension is:

$$T=2F_{AB}\frac{s_X-L_{BB}}{l_{AB}}+2F_{AC}\frac{s_X}{l_{AC}} \quad (2)$$

The kinematics of the structure defines: $l_0=\frac{1}{2}\sqrt{(L_0-s_0)^2+s_0^2+L_0^2}$, with $l_{AB} = l_{Ac} = l_{BC} = l_0$, $L_{AA} = L_{BB} = L_{CC} = L_0$, $s_X = s_Y = s_Z = L_0/2$, $s_0 = L_0/2$ and $l_0=\sqrt{3/8L_0}$ for initial evaluation. If we assume that the filaments are linearly elastic of stiffness ***k*** and resting length l_r. The force then in each actin filament and the intermediate filament is given by:

$$F=\begin{cases} k(l-l_r) & l>l_r \\ 0 & l<l_r \end{cases} \quad (3)$$

This relationship can also be extended to second order with $F = k(l-l_r)^2$ for the intermediate filaments. Based on equations (2) (3) and the kinematics, the relationship of ***T*** and s_X can be obtained. The derivation of the model without the intermediate filament has been thoroughly discussed in (27). A similar approach can be applied to the configuration with the filament and a new relationship of ***T*** and s_X can be found. The derivative of them can be evaluated at the initial condition and we have E^* expressed in the initial length of the actin filament/microtubule (L_0/l_0), the initial force in the actin filament (F_0) and intermediate filament (F_1), and the initial strain in the filament (ε_0).The initial forces in the actin filament and the intermediate filament were generated by the force generating proteins, such as actomyosin motors. These can be found in the literature, as shown in Tab. 1.

Results

AFM nanorobotics mechanically disrupts intercellular adhesion

There have been reports of nanodissection *on fixed* rat aortic smooth muscle cells (14) and mouse endothelial cells (13); in both cases, a ‘scar’ was created successfully on top of the cell surface. The dissection of *live* cells proves to be more complicated than fixed cells. Once fixed, the polymeric structure of the cell membrane as well as the cytoskeleton will be cross-linked, evidenced by the large increase of stiffness of fixed cells (28). Thus, fixed cellular bodies can be regarded as a single material structure. However, live cells display distinct mechanical properties, elasticity in their delicate membrane and the cytoskeleton structure and viscosity in their cytoplasm. It was shown that intermediate filaments have extremely high tensile strength by AFM stretching (10, 29, 30). Therefore, it behaves as a composite material structure. To dissect the intermediate filament network inside the cell poses larger challenges (illustrated in Figure 3A). The cell body will deform when the AFM probe is pushed against the membrane. A tip that is sharp enough is required to penetrate the cell membrane before it reaches the cytoplasm and the intermediate filaments. Although a

high-aspect ratio probe is desirable, it is not a necessity as we proved in our experiments. We used a pyramid silicon nitride probe with a tip apex diameter of 2 nm for the nanosurgery.

The force displacement curve in Figure 3C shows the entire process when the probe was driven towards the cell membrane until it penetrated the cell membrane, compared with the process without penetration in Figure 3B. This begins with the contact point denoted as a circle when the probe starts to deform the cell membrane and when the laser detector starts to detect vertical deflection. Subsequently, at a certain point when tip deflection is large enough, the probe generates a normal force to penetrate the cell membrane. The penetration force was observed when there was a sharp drop of repulsive force indicating a smaller resistance of cytoplasm compared with the cell membrane. The measured penetration force for keratinocytes is approximately 1.9 ± 0.5 nN, similar value as reported in some other cell penetration experiments(31, 32). The distance travelled by the vertical piezo actuator between the contact point and penetration point can be used as a guide to set the overall cutting depth for the nanomanipulation operation.

Force measurement has been applied in investigations of biological process. Most of these applications focused on the normal force obtained from vertical deflection of the cantilever. We controlled the lateral force to cut through the elastic filament structures. By maintaining a constant normal force and moving the cantilever horizontally, the lateral deflection of the cantilever can be obtained (as illustrated in Figure 4A) from the PSD signal. The normal force applied to the cantilever was determined by the depth of penetration and depth of probe contacting the substrate underneath as measured by force displacement.

The lateral position of the probe was determined by a pre-defined trajectory around a specific cell shown as the three dimensional construction of the original image from the custom-made software in Figure 4C. When moving along the trajectory, at each time t, the cutting force in the planar direction can be determined by $F = F_l / \cos(\theta)$, where F_l is the lateral force due to the twist of the cantilever perpendicular to its longitude direction and $\theta = a \tan 2(y,x)$ is the angle at each position (x,y) (illustrated in Figure 4B). The detailed force model and calibration can be found in our previous work (33). The trajectory was then translated to position information, which directs the lateral movement of the probe.

A real time measurement data is shown in Figure 4D, in which the XY position, the cutting force F and the Z cutting depth were recorded. Three repeated cutting procedures were performed, the lateral movement is at 1.2 μm/s maximum for both X and Y; while a constant Z position is maintained immediately when the probe engages with the cell sample, therefore to apply a constant normal force for the lateral cutting force to take effect. The maximum cutting force recorded during the operation was around 18 nN. Similar force profile was observed for all three cutting procedures, it was maintained at a higher level less than 20 nN for about 2 seconds before being lowered to around 7-10 nN. The larger force was due to the higher topography in the first phase of the travel, and more bundles of filament pose a larger resistance. Sudden release of forces to extreme low levels, or spikes, in the force profile should be caused by the snap of bundles of intermediate filaments. Overall, the lateral force was greater than reported on single strand intermediate filament

stretching (29). This could be due to the fact that bundles of intermediate filament were stretched and severed. Besides, the anchoring of intermediate filament through the cytoskeleton network would increase the tension in the filament. This was echoed by the shorter stretching length of the filament Δl=148 nm and the distance between two bundles d=360 nm shown in the insect of Figure 4D.

Images in Figure 5A and B show the image before and after three repetitions of nanosurgery with a cutting depth of 100 nm. A line segment section at the working area shows the topographical change in Figure 5C and D. The filament structures were severed as indicated by the height decrease in the topography image, and the dissection was controlled within 300 nm. The severing was successfully completed indicated by the structural rearrangement of the cytoskeleton. Due to the pre-defined cutting depth, the structures at the lower topography area were not affected. The stiffness data was collected before and after the dissection operations, which cut off the connections between neighboring cells through repetitions of nanosurgery. The Young's modulus value dropped from 36.1 ± 3.5 kPa to 18.4 ± 1.9 kPa (Figure 6A and B). The well-connected cells are approximately 1.5-2 times stiffer than the cells whose intermediate filaments are cut loose thus lose their anchoring point from neighboring cells. Nanosurgery operations were also performed to sever the intermediate filament differently on varied locations on the cell. The result shows that they do have different impact on the cell structural arrangements and thus resulted in different changes of cell elasticity (Supplemental Material). Trypan blue staining showed that the cells are still alive after nanosurgery operations.

Pathogenic autoimmune antibody destroys the intercellular adhesion

Desmosomal cadherins are the pathophysiological targets of auto-antibodies in several blistering skin disorders. PV is a prototypical organ-specific autoimmune blistering skin disease that has been associated with the presence of auto-antibodies directed against the desmosomal molecules Dsg3 and in many cases also Dsg1 (19). The damaged desmosome leads to the disruption of cell-cell adhesion, detachment of neighboring keratinocyte cells from each other and eventually causes blistering of the skin. The effect of the autoimmune antibody was experimentally tested *in vitro* by applying it to the keratinocyte cell line. We have reported previously the structural transformation after treatment of this pathological antibody to keratinocytes that mimics the disease states (20). The detailed structure from combined imaging of AFM with Fluorescence Microscopy (FM) of intercellular junction showed the disappearance of junction material as well as retracted intermediate filaments. Nanomechanical analysis was carried out by AFM based nanoindentation before and after antibody treatment. The topographical change is echoed by the decrease of the cell stiffness as measured by AFM based nanoindentation. The Young's modulus value of normal cells dropped 36.2 ± 4.7 to 19.1 ± 3.9 kPa for pathogenic antibody treated cells as shown in Figure 6C.

Destruction of intermediate filaments by Calcium depletion results in decreased stiffness

The formation of desmosome requires the presence of Ca^{2+} in the growth medium, as Ca^{2+} forms covalent bonds with the desmosomal protein Dsg. By depleting the Ca^{2+} in the growth medium, the formation of desmosomes can be interrupted. The size and height

difference between normal cells and Ca^{2+} -depleted cells was analyzed as shown in Figure 6D and E. Normal cells display an intact intercellular junction, while the Ca^{2+}-depleted cells show an enlarged spacing between individual cells and they are all isolated from each other. Normal cells are stretched with a diameter 24.3 ± 4.8 μm and a height around 1.3 ± 0.3 μm; while Ca^{2+} -depleted cells are rounded up with a diameter 11.7 ± 2.1 μm and a cell height of 3.1 ± 0.7 μm (5 cells). The stiffness of both cells were also measured and compared, and the Young's modulus values agree well with previous measurements for normal cells and antibody treated cells. The stiffness decreases from 36.2 ± 4.7 kPa to around 18.2 ± 3.7 kPa for normal and Ca^{2+} -depleted cells as shown in Figure 6C.

Discussion

Both mechanical and biochemical modulations of desmosome yielded a cell sample without cell-cell adhesion, and in all case the cells display a decrease in stiffness. These data indicate that the loss of cell-cell adhesion either through mechanical dissection of intermediate filaments, or through desmosome disruption results in the loss of cell stiffness. Conceptually, when cells are modeled as tensegrity structure, pre-stress becomes the main characteristics that determines the stiffness of the cytoskeleton structure; it has been well documented that cells will become stiffer when pre-stress increases (34-37). Similar conditions for the keratinocytes are seen when their intermediate filaments are damaged. Since the intermediate filaments are tensional elements in the cytoskeleton system, the loss of tension due to the loss of intermediate filament- based adhesions either from antibody binding, calcium depletion, or mechanical dissection, lowers the pre-stress in the tensional elements, and therefore the stiffness. Theoretical calculation was then performed to verify the stiffness change with and without intermediate filaments in the structural model to confirm if the dissection operation was successfully achieved.

The plotting in Figure 6F shows the comparison of Young's modulus values with respect to the strain for configurations of with and without intermediate filaments using parameters in Table 1. The Young's modulus of cells with intermediate filaments modeled as linear force-deformation relationship in the configuration increased 19 percent at the upper boundary; even the less sensitive quadratic force-deformation relationship could yield higher Young's modulus values than that without intermediate filament in the configuration. The trend is also indicative of the contribution from the intermediate filaments, i.e., when the strain increases, the stiffness difference is larger. This agrees well with the functional contribution of intermediate filaments in the cytoskeleton system. They are responsible for the maintaining the shape when there is larger strain or deformation. As with these parameters, the absolute value of the Young's modulus shows discrepancy with the experiment, since the actual AFM measurement data is subject to a number of factors. Note that the average force in the actin filament can go up to 2 nN (38), which may well be the case in the typically-tough skin cells and would significantly increase the value of the Young's modulus in the simulation. Nevertheless, the trend predicted by the simulation shows the stiffening effect with the intermediate filament and the decrease thereof due to the loss of it, which confirms the successful nanodissection of intermediate filament connections between neighboring cells. The mechanical model was developed based on the tensegrity structure to show qualitatively that the cell behavior after cell adhesion loss of different mechanisms obeys the

biological laws that govern these biomechanical changes. Indeed, as we saw from the simulation, cells would display decreased stiffness when the treatments reduce the stress in the cell cytoskeleton structure and thus change to low stiffness equilibrium.

The mechanical cutting with a nanoscale scalpel provides a non-invasive surgical procedure rather than a chemical treatment, where location-specificity cannot be easily achieved. Moreover, the chemical methods that result in adhesiolysis are most likely to trigger a series of signaling cascades (39) that may lead to the other changes to the cell, side effects that confound experimental interpretation. The nanosurgery results in similar mechanical property changes as with the biochemical modulations, providing evidence that the intermediate filaments serve as one of the important elements in the maintaining of mechanical integrity of the cell structure.

In this study, we demonstrated that intercellular adhesion is one of the main mechanisms employed by epithelial cells to achieve functional homeostatis, using live keratinocytes as the model system to study this cellular behavior. We employed mechanical disruption with nanorobotic surgery to dissect intermediate filament structures between neighboring cells in order to mimic the effects of pathogenic antibody treatment and calcium depletion. Our findings applying nanosurgical manipulation to living cells have broad biological implications for the investigation of molecular and cellular function in physiologic and disease states, and for envisioning novel therapeutic strategies that involve manipulating or removing undesirable (eg. autoimmune or cancerous) cells.

Acknowledgments

This work was supported by NSF Grants IIS-0713346 and DMI-0500372, ONR Grants N00014-04-1-0799 and N00014-07-1-0935, and NIH Grant R43 GM084520.

References

1. Camarillo DB, Krummel TM, Salisbury JK Jr. Robotic technology in surgery: past, present, and future. Am J Surg. 2004 Oct; 188(4A Suppl):2S–15S. [PubMed: 15476646]
2. Kohli V, Elezzabi AY. Prospects and developments in cell and embryo laser nanosurgery. Wires Nanomed Nanobi. 2009 Jan-Feb;1(1):11–25.
3. Binnig G, Quate CF, Gerber C. Atomic Force Microscope. Phys Rev Lett. 1986 Mar 3; 56(9):930–3. [PubMed: 10033323]
4. Horber JK, Miles MJ. Scanning probe evolution in biology. Science. 2003 Nov 7; 302(5647):1002–5. [PubMed: 14605360]
5. Muller DJ, Dufrene YF. Atomic force microscopy as a multifunctional molecular toolbox in nanobiotechnology. Nat Nanotechnol. 2008 May; 3(5):261–9. [PubMed: 18654521]
6. Xi, N.; Fung, CKM.; Yang, R.; Lai, KWC.; Wang, DH.; Seiffert-Sinha, K., et al. Atomic force microscopy as nanorobot Atomic Force Microscopy in Biomedical Research. Springer; 2011. p. 485-503.
7. Xi N, Song B, Yang R, Lai K, Chen H, Qu C, et al. Video Rate Atomic Force Microscopy (AFM) Using Compressive Scanning. IEEE Nanotechnology Magazine. 2013; 7(1):4–7.
8. Li G, Xi N, Wang DH. In situ sensing and manipulation of molecules in biological samples using a nanorobotic system. Nanomedicine. 2005 Mar; 1(1):31–40. [PubMed: 17292055]
9. Han SW, Nakamura C, Obataya I, Nakamura N, Miyake J. A molecular delivery system by using AFM and nanoneedle. Biosens Bioelectron. 2005 Apr 15; 20(10):2120–5. [PubMed: 15741084]

10. Kreplak L, Bar H, Leterrier JF, Herrmann H, Aebi U. Exploring the mechanical behavior of single intermediate filaments. J Mol Biol. 2005 Dec 2; 354(3):569–77. [PubMed: 16257415]
11. Wen CK, Goh MC. AFM nanodissection reveals internal structural details of single collagen fibrils. Nano Lett. 2004 Jan; 4(1):129–32.
12. Hoh JH, Lal R, John SA, Revel JP, Arnsdorf MF. Atomic Force Microscopy and Dissection of Gap-Junctions. Science. 1991 Sep 20; 253(5026):1405–8. [PubMed: 1910206]
13. Riethmuller C, Nasdala I, Vestweber D. Nano-surgery at the leukocyte-endothelial docking site. Pflug Arch Eur J Phy. 2008 Apr; 456(1):71–81.
14. Beard JD, Burbridge DJ, Moskalenko AV, Dudko O, Yarova PL, Smirnov SV, et al. An atomic force microscope nanoscalpel for nanolithography and biological applications. Nanotechnology. 2009 Nov 4.20(44)
15. Staple DB, Loparic M, Kreuzer HJ, Kreplak L. Stretching, Unfolding, and Deforming Protein Filaments Adsorbed at Solid-Liquid Interfaces Using the Tip of an Atomic-Force Microscope. Phys Rev Lett. 2009 Mar 27.102(12)
16. Green KJ, Simpson CL. Desmosomes: New perspectives on a classic. J Invest Dermatol. 2007 Nov; 127(11):2499–515. [PubMed: 17934502]
17. Godsel LM, Hobbs RP, Green KJ. Intermediate filament assembly: dynamics to disease. Trends Cell Biol. 2008 Jan; 18(1):28–37. [PubMed: 18083519]
18. Kowalczyk AP, Bornslaeger EA, Norvell SM, Palka HL, Green KJ. Desmosomes: intercellular adhesive junctions specialized for attachment of intermediate filaments. International review of cytology. 1998; 185:237–302. [PubMed: 9750269]
19. Payne AS, Hanakawa Y, Amagai M, Stanley JR. Desmosomes and disease: pemphigus and bullous impetigo. Curr Opin Cell Biol. 2004 Oct; 16(5):536–43. [PubMed: 15363804]
20. Fung CKM, Seiffert-Sinha K, Lai KWC, Yang RG, Panyard D, Zhang JB, et al. Investigation of human keratinocyte cell adhesion using atomic force microscopy. Nanomed-Nanotechnol. 2010 Feb; 6(1):191–200.
21. Fung CKM, Ning X, Ruiguo Y, Seiffert-Sinha K, King Wai Chiu L, Sinha AA. Quantitative Analysis of Human Keratinocyte Cell Elasticity Using Atomic Force Microscopy (AFM). NanoBioscience, IEEE Transactions on. 2011; 10(1):9–15.
22. Ingber DE. Tensegrity I, Cell structure and hierarchical systems biology. Journal of Cell Science. 2003 Apr 1; 116(Pt 7):1157–73. [PubMed: 12615960]
23. Ingber DE. Tensegrity II. How structural networks influence cellular information processing networks. Journal of Cell Science. 2003 Apr 15; 116(Pt 8):1397–408. [PubMed: 12640025]
24. Ingber DE. Mechanosensation through integrins: Cells act locally but think globally. P Natl Acad Sci USA. 2003 Feb 18; 100(4):1472–4.
25. Maniotis AJ, Chen CS, Ingber DE. Demonstration of mechanical connections between integrins cytoskeletal filaments, and nucleoplasm that stabilize nuclear structure. P Natl Acad Sci USA. 1997 Feb 4; 94(3):849–54.
26. Yang, R.; Xi, N.; Lai, KWC.; Gao, B.; Chen, H.; Su, C., et al. Motion controller for the Atomic Force Microscopy based nanomanipulation system. IEEE/RSJ International Conference on Intelligent Robots and Systems; 2009; p. 1339-44.
27. Stamenović D, Fredberg JJ, Wang N, Butler JP, Ingber DE. A microstructural approach to cytoskeletal mechanics based on tensegrity. Journal of Theoretical Biology. 1996; 181(2):125–36. [PubMed: 8935591]
28. Kuznetsova TG, Starodubtseva MN, Yegorenkov NI, Chizhik SA, Zhdanov RI. Atomic force microscopy probing of cell elasticity. Micron. 2007; 38(8):824–33. [PubMed: 17709250]
29. Kreplak L, Herrmann H, Aebi U. Tensile properties of single desmin intermediate filaments. Biophys J. 2008 Apr 1; 94(7):2790–9. [PubMed: 18178641]
30. Qin Z, Kreplak L, Buehler MJ. Nanomechanical properties of vimentin intermediate filament dimers. Nanotechnology. 2009 Oct 21.20(42)
31. Obataya I, Nakamura C, Han S, Nakamura N, Miyake J. Nanoscale operation of a living cell using an atomic force microscope with a nanoneedle. Nano Lett. 2005 Jan; 5(1):27–30. [PubMed: 15792407]

32. Han SW, Nakamura C, Kotobuki N, Obataya I, Ohgushi H, Nagamune T, et al. High-efficiency DNA injection into a single human mesenchymal stem cell using a nanoneedle and atomic force microscopy. Nanomed-Nanotechnol. 2008 Sep; 4(3):215–25.
33. Li GY, Xi N, Yu MM, Fung WK. Development of augmented reality system for AFM-based nanomanipulation. Ieee-Asme T Mech. 2004 Jun; 9(2):358–65.
34. Wang N, Tolic-Norrelykke IM, Chen J, Mijailovich SM, Butler JP, Fredberg JJ, et al. Cell prestress. I. Stiffness and prestress are closely associated in adherent contractile cells. Am J Physiol Cell Physiol. 2002 Mar; 282(3):C606–16. [PubMed: 11832346]
35. Stamenovic D, Mijailovich SM, Tolic-Norrelykke IM, Chen J, Wang N. Cell prestress. II. Contribution of microtubules. Am J Physiol Cell Physiol. 2002 Mar; 282(3):C617–24. [PubMed: 11832347]
36. Hu S, Chen J, Wang N. Cell spreading controls balance of prestress by microtubules and extracellular matrix. Front Biosci. 2004 Sep 1.9:2177–82. [PubMed: 15353279]
37. Fereol S, Fodil R, Laurent VM, Balland M, Louis B, Pelle G, et al. Prestress and adhesion site dynamics control cell sensitivity to extracellular stiffness. Biophys J. 2009 Mar 4; 96(5):2009–22. [PubMed: 19254561]
38. Shin JH, Tam BK, Brau RR, Lang MJ, Mahadevan L, Matsudaira P. Force of an actin spring. Biophys J. 2007 May 15; 92(10):3729–33. [PubMed: 17351007]
39. Wang X, Bregegere F, Frušić-Zlotkin M, Feinmesser M, Michel B, Milner Y. Possible apoptotic mechanism in epidermal cell acantholysis induced by pemphigus vulgaris autoimmunoglobulins. Apoptosis. 2004; 9(2):131–43. [PubMed: 15004510]
40. Qin Z, Kreplak L, Buehler MJ. Nanomechanical properties of vimentin intermediate filament dimers. Nanotechnology. 2009 Oct 21.20(42):425101. [PubMed: 19779230]
41. Sept D, Xu J, Pollard TD, McCammon JA. Annealing accounts for the length of actin filaments formed by spontaneous polymerization. Biophys J. 1999 Dec; 77(6):2911–9. [PubMed: 10585915]
42. Takagi Y, Homsher EE, Goldman YE, Shuman H. Force generation in single conventional actomyosin complexes under high dynamic load. Biophys J. 2006 Feb 15; 90(4):1295–307. [PubMed: 16326899]

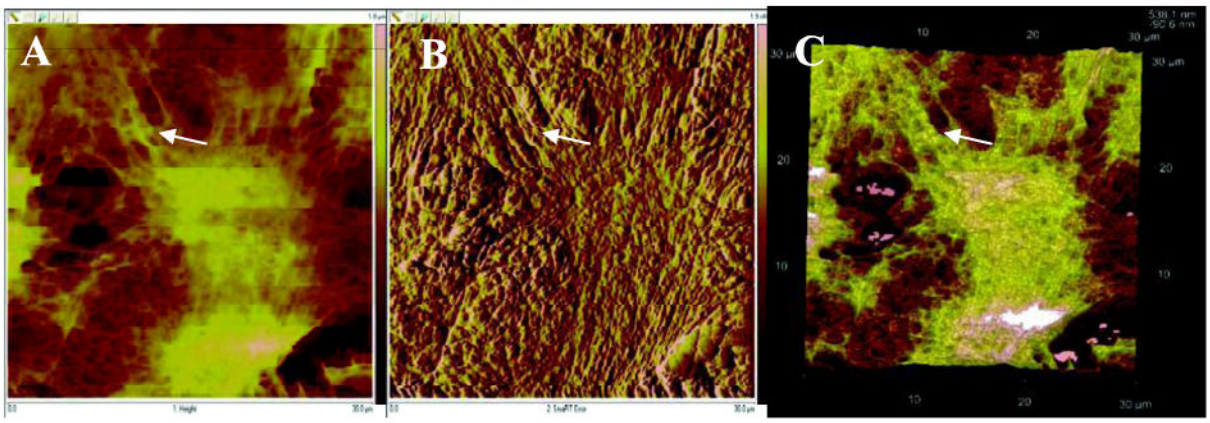

Figure 1.

Intermediate filament bundles imaged with AFM show stranded filamentous structures at the peripheral of the cells (arrows). A: Topography image, B: Deflection error image, C: Three dimensional rendering. Scan size: 30 μm.

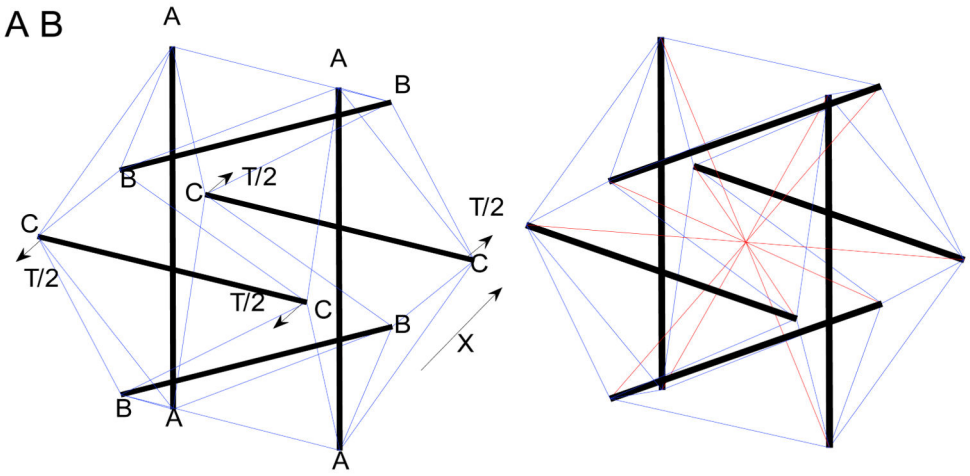

Figure 2.

The tensegrity structure with 6 compressional (black) and 24 tensional (blue) elements was used to model the cell stiffness with (**A**) and without **(B)** the intermediate filament which is considered tensional elements (red) projecting from the nucleus to the cell peripheral.

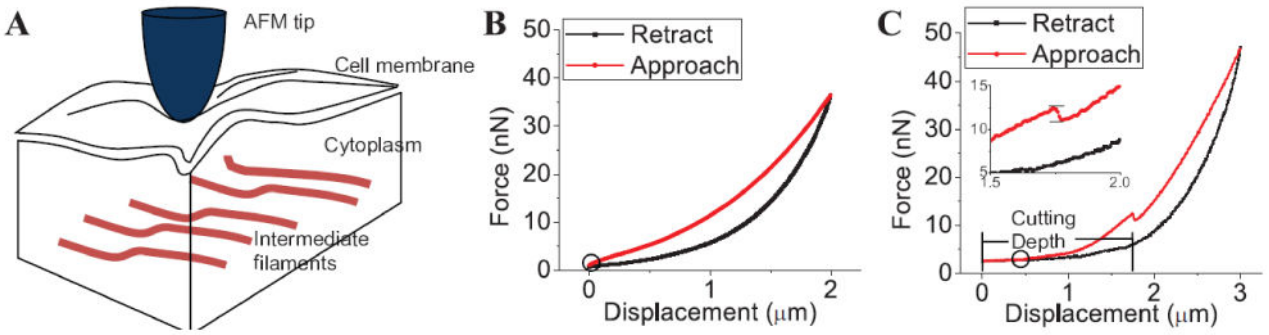

Figure 3.

(A) Illustration of composite cell structure during cell indentation and dissection; **(B)** Force-displacement curve without penetration of the cell membrane; **(C)** Force displacement curve with penetration of the cell membrane with the kink, indicating the force drop, zoomed-in in the inset, a 1.9 nN penetration force was observed.

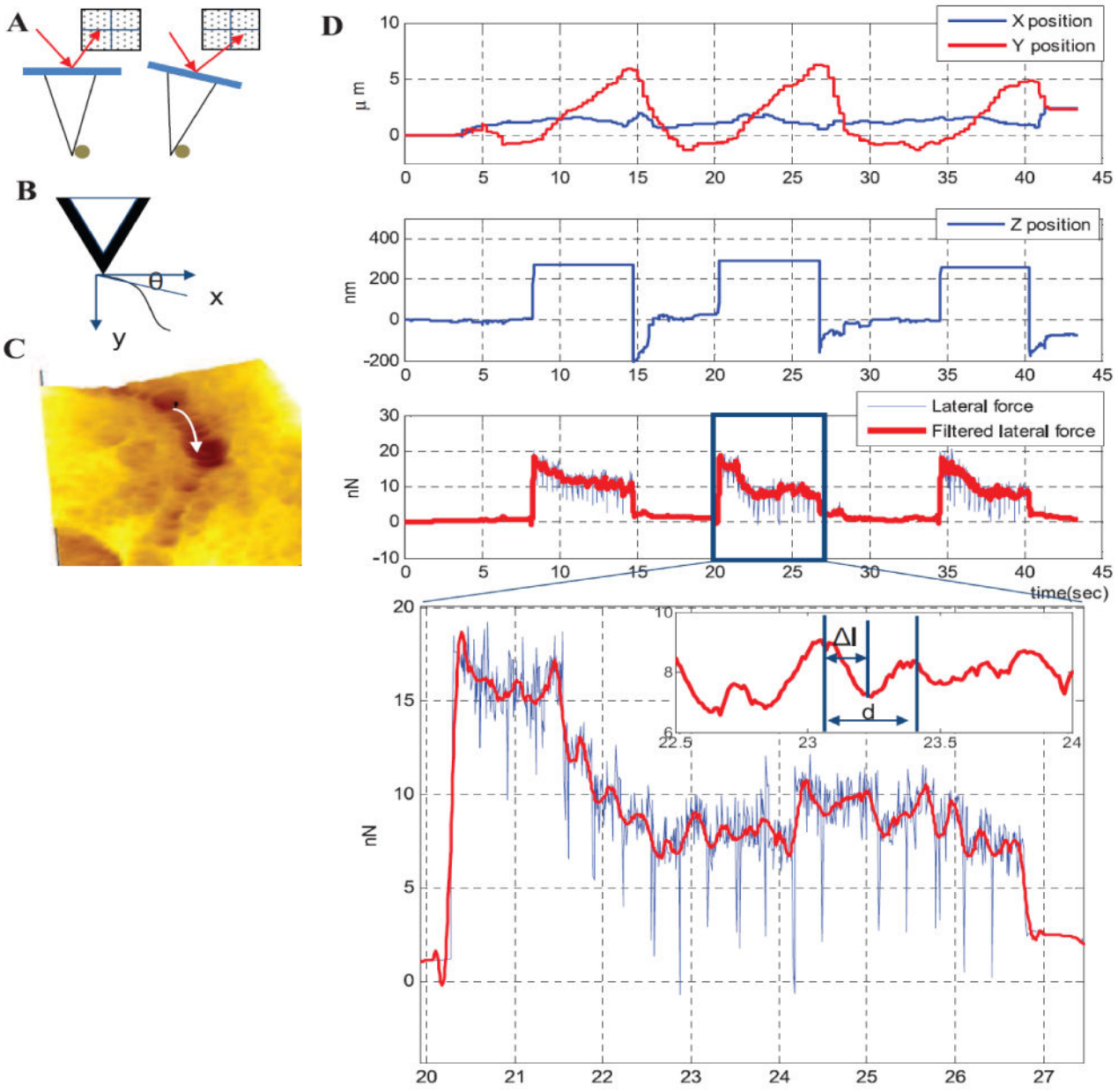

Figure 4.

(**A**) The lateral force was the laser position shift in the horizontal direction on the detector; (**B**) The tangent direction of the trajectory defines the angle (θ) between the cutting force *F* and the lateral force F_n; (**C**) The trajectory of the nanosurgery on the cell periphery between neighboring cells with the black triangle indicating the tip position, the 3D structure was recreated from the AFM image obtained before nanosurgery using custom-made nanomanipulation software; (**D**) the X, Y, Z piezo position and the cutting force *F* in the process of the nanosurgery along the path in (**C**). Three repetitions of dissection operation were recorded with a cutting depth of 100 nm. The detailed force profile is magnified with the insect showing the stretching distance Δ*l*=148 nm and the distance between two strands of filaments *d*=360 nm.

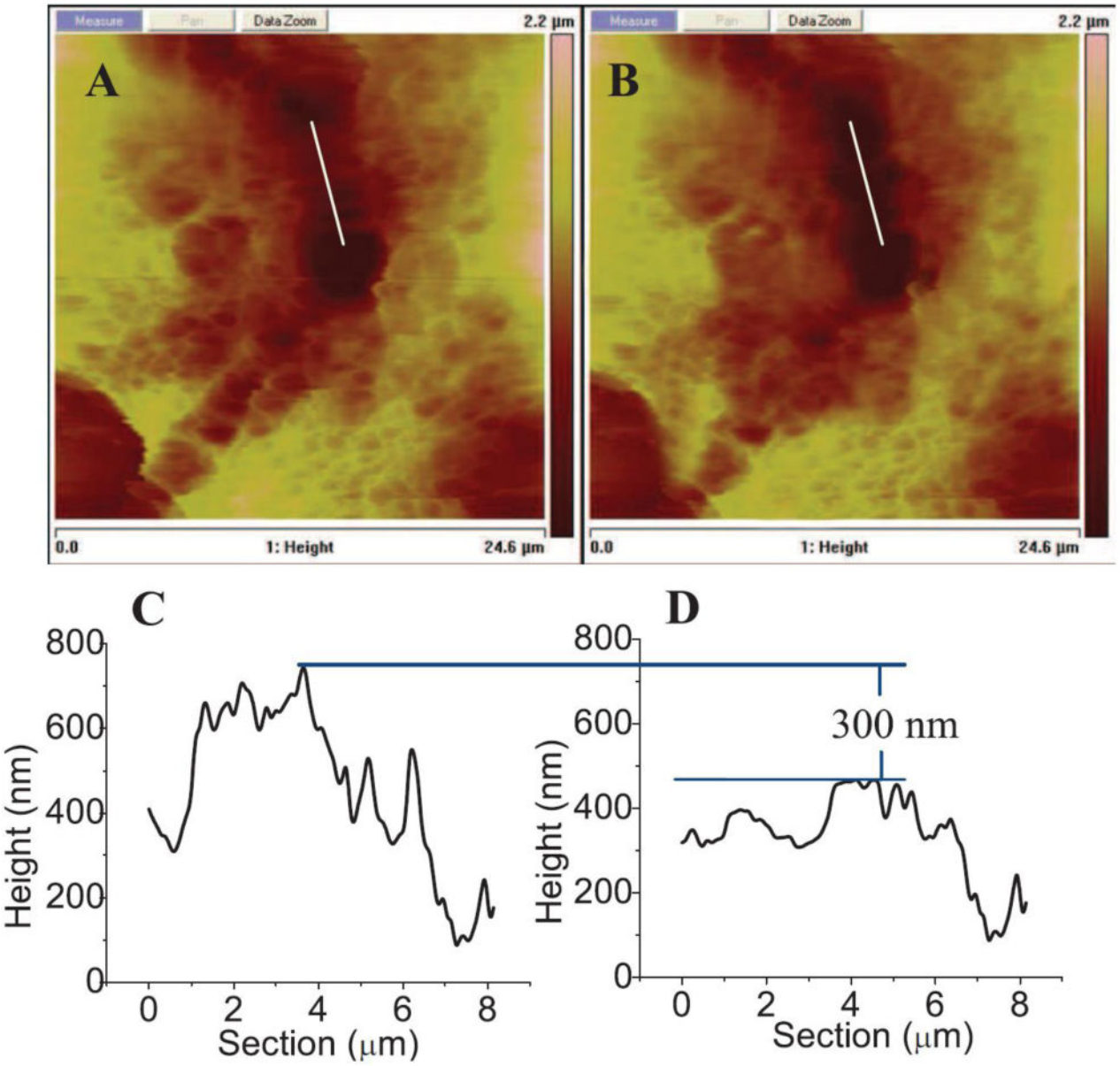

Figure 5.

(**A**), (**B**) The AFM image of keratinocyte cells before and after three repeating nanosurgeries (scan size: 24.5 µm); **(C), (D)** the height information of the line section indicated in (**A**)(B) before and after nanosurgery along the trajectory in Figure 4 shows the detailed structural change. The severing was successfully completed indicated by the structural rearrangement of the cytoskeleton, since the pre-defined cutting depth, the structures at the lower topography area was not affected.

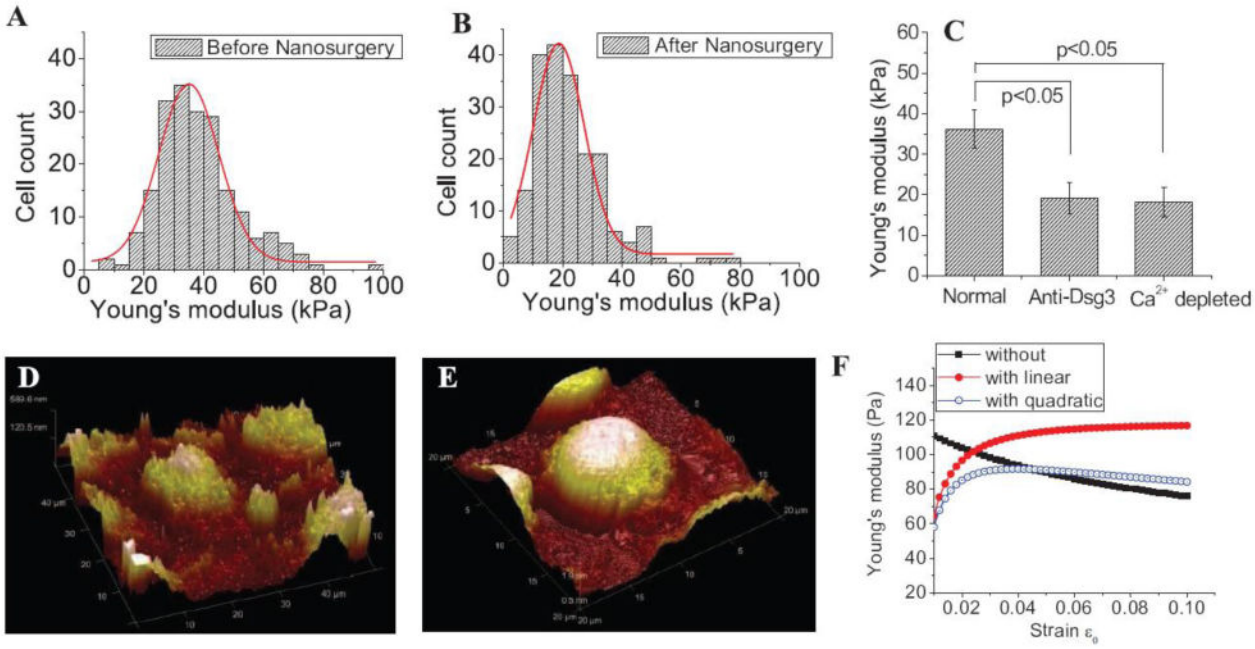

Figure 6.

(A) The stiffness change of individual cells before ten repetitions of nanosurgery with cutting depth of 100 nm each and after a 3 hour continuous observation; **(B)** the stiffness drop was assessed statistically before and after nanosurgery from 36.1± 3.5 kPa to 18.4 ± 1.9 kPa (mean ± SEM, n=200). **(C)** The stiffness drop was observed for anti-Dsg3 antibody treated samples and the Ca^{2+} depleted samples; **(D)** the normal keratinocyte cell structure and **(E)** the cell structure after non-formation of desmosomes. **(F)** The stiffness comparison with and without intermediate filament over strain; a significant drop of stiffness was observed without intermediate filament connection.

Table 1
Parameter list for the numerical simulation

Variable	Physical meaning	value	unit	Reference
F_0	Average force generated by a single actomyosin motor	10	pN	(38)
F_1	Average force generated by a single intermediate filament	3.2	nN	(40)
L_0	Estimated length of an actin filament from volume fraction	7	μm	(41)
K	The linear stiffness coefficient of an actin filament	0.05	pN/nm	(42)
K_1	The linear stiffness coefficient of an intermediate filament	0.10	pN/nm	(40)